Electronic structure at the perylene-tetracarboxylic acid dianhydride/Ag(111) interface studied with two-photon photoelectron spectroscopy

Sönke Sachs,[1] Christian H. Schwalb,[2] Manuel Marks,[2] Achim Schöll,[1,a)] Friedrich Reinert,[1] Eberhard Umbach,[1] and Ulrich Höfer[2]
[1]*Universität Würzburg, Experimentelle Physik II, Am Hubland, D-97074 Würzburg, Germany*
[2]*Fachbereich Physik und Zentrum für Materialwissenschaften, Philipps-Universität, D-35032 Marburg, Germany*

(Received 18 May 2009; accepted 16 September 2009; published online 9 October 2009)

The electronic structure of the prototype metal/organic contact 3,4,9,10-perylene-tetracarboxylic acid dianhydride (PTCDA) on a Ag(111)-surface has been investigated using time- and angle-resolved two-photon photoelectron spectroscopy (2PPE). Our analysis addresses particularly the nature of the interface state (IS) emerging at the interface due to the substrate-adsorbate interaction [C. H. Schwalb, S. Sachs, M. Marks *et al.*, Phys. Rev. Lett. **101**, 146801 (2008)]. Its free-electron-like dispersion and a possible backfolding at the surface Brillouin zone boundaries are discussed. Time-resolved pump-probe experiments reveal the inelastic electron lifetime along the dispersion parabola and show its decrease for increasing parallel momentum. The temperature dependence of the peak linewidth indicates a coupling of the IS to molecular vibrations. Moreover, additional aspects are addressed, such as the determination of the electron attenuation length of photoelectrons for low kinetic energy originating from the IS and the work function change of the sample upon PTCDA adsorption with very high energy resolution. © *2009 American Institute of Physics*. [doi:10.1063/1.3243851]

I. INTRODUCTION

Various applications of π-conjugated molecules in molecular electronic devices entered the market (like organic light emitting diodes and displays) or are becoming feasible (like organic field effect transistors and organic photovoltaic cells), thus motivating the large research interest in the field of organic thin films. In this context the interface between the molecules in the active layer and metal contacts is of crucial importance since it decisively determines the device performance. Electronic structure, static charge transfer and injection mechanisms at these contacts, and their dependence on the system parameters are of great interest.[1] On the other hand, the investigation and understanding of the fundamental mechanisms of the interaction of π-conjugated molecules with metals are challenging questions in the field of surface science, since these combined molecule-metal systems are of a complexity that is at the frontier of experimental and theoretical possibilities.

With respect to fundamental research the molecule 3,4,9,10-perylene-tetracarboxylic acid dianhydride (PTCDA) has been studied extensively with a large variety of experimental and theoretical methods.[2–6] The adsorption of PTCDA on Ag(111) is particularly interesting because the strength of the interaction is clearly chemisorptive,[5] although single adsorbed molecules are still very mobile on the surface and move over distances of micrometers.[7] PTCDA monolayers (ML) on Ag(111) arrange in a highly ordered herringbone structure similar to the crystal planes of bulk PTCDA. Hence a highly ordered growth beyond the first monolayer is observed.[8] The electronic structure of PTCDA monolayers on Ag(111), however, differs significantly from the bulk electronic structure. Particularly, the bulk lowest unoccupied molecular orbital (LUMO) hybridizes with the Ag *sp*-band and consequently is downshifted below the Fermi energy (E_F) and partly occupied. Furthermore, the highest occupied molecular orbital (HOMO), LUMO+1, and LUMO+2 are also altered upon adsorption.[4] Recently a strongly dispersing interface state (IS) was found,[9] which was identified with two-photon photoemission spectroscopy (2PPE) to originate mainly from the Ag(111) Shockley state (SS).[10] The lifetime of 54 fs for the IS is relatively short for a state located only 0.6 eV above E_F. The IS must therefore have a large penetration into the metal. On the adsorbate side, its wave function penetrates the PTCDA beyond the monolayer.[10] Due to the chemisorption a contribution of the molecular layer to the IS is possible, especially for high $k_{\parallel}$,[9,10] but could not be identified clearly. 2PPE experiments with PTCDA films of varying morphologies on Ag(111) revealed that the properties of the IS state depend sensitively on film structure and adsorbate-substrate interaction.[11]

In this paper, the electronic structure of the PTCDA/Ag(111) interface is characterized in detail with 2PPE. 2PPE gives access to the energetics and dispersion of electronic states, probing both occupied and unoccupied electronic states in the vicinity of E_F with high energy resolution. An important advantage is the ability to investigate the dynamics of unoccupied states by exciting electrons into the state in a first step and emitting them with a second time-delayed photon. It has been used for detailed studies of ultrafast electron dynamics at the surfaces of semiconductors[12–15] and

a)Electronic mail: achim.schoell@physik.uni-wuerzburg.de.

metals,[16–20] as well as for a variety of adsorbate layers.[1,21–25] First, we discuss the excitation schemes used for our 2PPE-experiments. In the following the change in the work function upon PTCDA adsorption is investigated with very high accuracy and a clear effect of the peculiar electronic structure of the PTCDA monolayer can be identified. Experimental evidence for the location of the IS at the interface is given and the electron attenuation length for low kinetic energy electrons originating from the IS is determined additionally by analyzing 2PPE spectra from films of different thickness. Photon energy dependent spectra reveal the unoccupied nature of the IS. The dispersion of the IS is discussed. In particular the possible backfolding of the IS band at the PTCDA surface Brillouin zone (SBZ) boundaries indicates a substrate-adsorbate interaction affecting the IS. After that, the decay of the electron population of the IS is studied depending on the parallel momentum $k_{\parallel}$ for 1 and 2 ML films. The temperature dependence of the IS linewidth indicates relatively strong electron-phonon coupling.

II. EXPERIMENTAL

The 2PPE experiments were carried out in two different ultrahigh vacuum systems with base pressures below 1×10^{-10} mbar. The first UHV-photoemission experiment, in the following called PE-I, is equipped with a hemispherical energy analyzer (VSW HSA 150) and a one-dimensional five-channeltron-array detector. At the PE-I chamber a Ti:sapphire oscillator with a repetition rate of 82 MHz was used as laser source. The high flexibility of different two color excitation schemes is achieved by second harmonic generation and sum frequency generation of the fundamental beam ($\hbar\omega_{\mathrm{IR}}=1.56$ eV, 45 fs pulses), resulting in 47 fs pulses at $\hbar\omega_{\mathrm{Blue}}=3.10$ eV and 70 fs pulses with an energy of $\hbar\omega_{\mathrm{UV}}=4.70$ eV. The maximum of the overall energy resolution of the PE-I was 22 meV including the laser linewidth, with the maximal angular resolution of 1.4°. Dispersion measurements are realized by rotating the sample and calculating the momentum of the electrons parallel to the surface using $\hbar k_{\parallel}=\sqrt{2m_eE_{\mathrm{kin}}}\sin(\vartheta)$, where ϑ is the angle between the surface normal of the sample and the energy analyzer.

Some of the dispersion measurements presented in this paper were performed at a second 2PPE setup equipped with a two-dimensional detector with an angle-resolved lens mode (Specs Phoibos 150),[26] henceforth called PE-II. The analyzer allows conformal imaging of the parallel momentum of the photoemitted electrons and therefore gives a direct image of the band structure of the sample SBZ around $\bar{\Gamma}$. The laser system used at the PE-II UHV-chamber is a commercial regenerative amplifier system (Coherent RegA 9050). An optic parametric oscillator (Coherent OPA 9450) and subsequent frequency doubling yield pulses with energies of $\hbar\omega_{\mathrm{Green}}=2.33$ eV for the fundamental beam and $\hbar\omega_{\mathrm{UV}}=4.66$ eV for the second harmonic photons at pulse durations of 50 and 58 fs, respectively. The resolution at this setup was determined to be 29 meV in energy including the laser linewidth and 0.4° angle.

The Ag(111) crystal was prepared with repeated cycles of Ar^+-sputtering and annealing. The cleanliness and structural order were subsequently checked with x-ray photoelectron spectroscopy (XPS) and low energy electron diffraction. PTCDA films were evaporated onto the substrate with a home-build Knudsen cell type evaporator with growth rates between 0.2 and 0.5 ML/min. The film thickness was determined from the calibrated evaporation rate and evaporation time and verified by XPS from the attenuation of the substrate Ag $3d$ signal. The resulting error bar for the PTCDA layer thickness can be estimated by 0.5 ML. Multilayer films were grown at a substrate temperature of 270 K, where layer-by-layer growth occurs. At this temperature the films grow as a mixture of α- and β-phases of bulk PTCDA.[8] Monolayer films were prepared by desorption of a multilayer film at temperatures of 540 K, resulting in a closed, long-range ordered monolayer. Unless otherwise noted, the spectroscopic experiments were performed at a temperature of 300 K.

In the following paragraphs two different energy notations will be used which differ by their reference point. The reference point for the kinetic energy E_{kin} of the photoemitted electrons is the vacuum level E_{Vac} of the sample. Final state energy E_{Final} means the energy of the photoelectrons with respect to the sample Fermi energy E_F. The difference between these two energy scales is the sample work function Φ: $E_{\mathrm{Final}}=E_{\mathrm{kin}}+\Phi$.

III. RESULTS AND DISCUSSIONS

A. Excitation schemes

The details of the 2PPE-spectra change with the applied photon energies in the experiment. So first these general properties of the 2PPE spectra will be discussed using excitation schemes applied at the PE-I, where most of the data presented in this paper have been recorded. As already mentioned different combinations of photon energies can be chosen. In detail, the combinations of frequency tripled and fundamental pulses UV/IR (4.66 eV/1.56 eV), frequency tripled and doubled pulses UV/blue (4.66 eV/3.10 eV) or only the third harmonic light UV/UV (4.66 eV/4.66 eV) are available. Time-resolved measurements can be realized with the combinations UV/IR and UV/blue. The PE-II excitation scheme UV/green (4.66 eV/2.33 eV) is similar to the UV/blue case and will therefore not be described in further detail.

In Fig. 1 the different excitation schemes for the 2PPE-experiments on PTCDA/Ag(111) are shown. With adsorption of the PTCDA-molecules the signal of the PTCDA/Ag(111) IS appears in the 2PPE-spectra.[10] Electrons excited into this state can only be photoemitted by high energetic UV-photons, as shown in Fig. 1. Therefore the emission scheme does not differ for the different energy combinations and the signal is always found at the same final state energy.

In addition to the IS, also the first two image-potential states ($n=1,2$) can be probed with the 2PPE-experiment. These states are bound with respect to the sample vacuum level E_{vac} formed due to an image-potential developing at the interface between two dielectric materials[27] and can only be occupied by UV-photons. The photoemission process is then performed by photon energies larger than the state's binding energy. Using IR-photons the electrons appear at a final state energy of about 5.4 eV and the signal of the $n=1$ image-

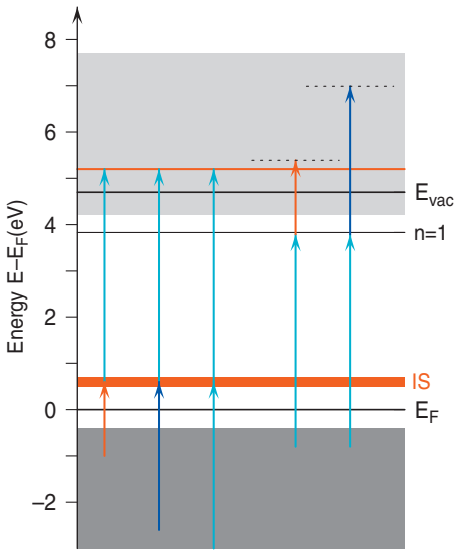

FIG. 1. Possible 2PPE-excitation schemes at the PE-I for the photon energy combinations UV/IR, UV/blue, and UV/UV for PTCDA/Ag(111). Depending on the photons used to photoemit electrons from the intermediate state, the signal is shifted in its final state energy. While the signal of the image-potential states (dashed lines) is shifted for the different excitation schemes due to different photon energies of the probe laser (blue, IR), the IS (thin solid line) is always probed by UV photons and its final state energy is hence independent from the applied photon combination (UV/IR, UV/blue, respectively). The combination UV/green used at PE-II is similar to the UV/blue case.

potential state superimposes with the IS electrons emitted by UV-photons which appear as a shoulder on the lower energy side. For photoemission via a second UV-photon the electrons are detected at a $\Delta\hbar\omega=\hbar\omega_{UV}-\hbar\omega_{IR}=3.14$ eV higher final state energy. The combination of UV- and blue-photons also shifts the image-potential signal away from the IS and additionally facilitates separate time-resolved measurements of all states.

Besides the changes in the relative photoemission yield from the different states due to varying excitation schemes and the shifted final state energies of the image-potential states, no significant modifications of the 2PPE-spectra are observed in the case of PTCDA/Ag(111). This leads to the conclusion that all photon energy combinations are equivalent and the excited electrons originate from occupied metallic states below E_F.

B. Work function

The work functions of the samples were determined by the low energy cutoff of the 2PPE spectra. The cutoffs are shown for the clean Ag(111) substrate and for various PTCDA film thicknesses ($\Theta=1$ to 13 ML) in Fig. 2(a). The peaks in the spectra consist of photoelectrons excited by one UV-photon from occupied metal and molecular states near E_F and of secondary electrons. The peak is cut on the low energy side by the work function leading to a distinctly asymmetric line shape. The work function is determined from the half maximum of the rising edge (see Fig. 2). It is well known that PTCDA adsorption can reorganize the silver surface considerably.[2] Consequently, depending on the preparation and the history of the Ag(111) sample, the work

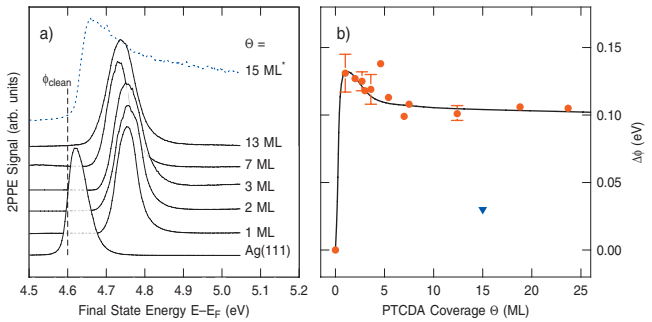

FIG. 2. Work function change upon PTCDA adsorption. (a) Series of normalized 2PPE spectra for the clean Ag(111) substrate and for samples with different PTCDA coverages recorded with PE-I using UV/UV excitation with a photon energy of $\hbar\omega_{UV}=4.69$ eV. The dashed spectrum represents a 15 ML film of inferior quality (see text). The workfunction Φ_{clean} of the clean Ag(111) sample is marked by the straight dashed line. (b) Relative shift of the work function $\Delta\Phi$ plotted against the PTCDA coverage with reference to the clean Ag(111) substrate. The spectra were measured with both setups, PE-I as well as PE-II. The triangle represents the work function of the dashed spectrum in (a).

function of the silver substrate varied in the range of 4.59–4.65 eV during our experiments. Figure 2(b) shows the work function change $\Delta\Phi$ relative to the respective clean Ag(111) work function determined before adsorption of PTCDA. Data for film thicknesses of 1 to 25 ML are presented. Samples of 1, 2, 3, and 12 ML were analyzed several times; for these samples the statistical variation of the determined work function change is shown as error bars. Upon adsorption of 1 ML the work function changes by $\Delta\Phi=130\pm10$ meV. The increase in the work function can be explained by the charge transfer from the metal to the molecules of the monolayer.[4,28] This charge transfer overcompensates effects that lower the work function, like the cushion effect.[28,29] Compared to other molecular adsorbate/metal systems, the observed work function change is small,[3,28] indicating only a small net charge redistribution at the interface. In the regime between 2 and (5–10) ML the work function decreases by 30 meV resulting in a relative change of $\Delta\Phi=100$ meV with respect to clean Ag(111). Beyond (5–10) ML the work function stays constant. Since the electronic structure of the PTCDA monolayer differs significantly from multilayers,[4] films between 2 and (5–10) ML can be associated with a transition regime between monolayer and bulk character. Another explanation for the relatively small work function drop can be found in the structure of the film. Since the films are grown at 300 K in a growth mode between Frank–van der Merve (layer by layer) and Stranski–Krastanov (layer+islands),[8] it is likely that the films roughen with increasing thickness. This roughening can significantly decrease the work function of thick films by values comparable to the experimental resolution, as we observed in our experiments for PTCDA films prepared with very high growth rates. The spectrum of such a sample with relatively low work function is shown in Fig. 2(a) as a dashed line.

The line shape of the leading edge at the low energy side of the spectra is determined by the experimental energy resolution as well as by the film morphology. In the case of films with higher roughness the measurement averages over a distribution of local differences in the work function. The

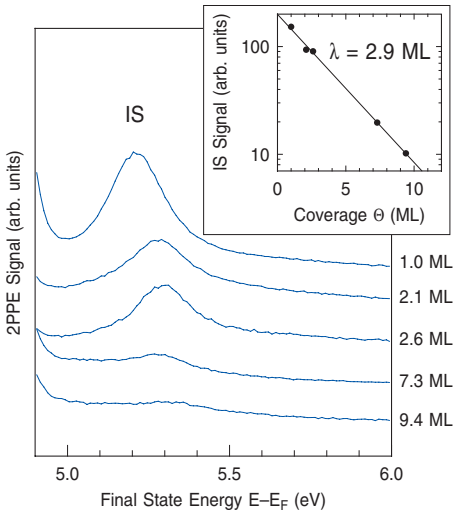

FIG. 3. Attenuation of the IS signal with increasing PTCDA film thickness. The integrated thickness dependent signal of the respective IS peaks is plotted against coverage as points in the inset. An exponential fit (straight line) yields an electron attenuation length of $\lambda = 2.9$ ML, which is equivalent to a mean free path of 9.3 Å.

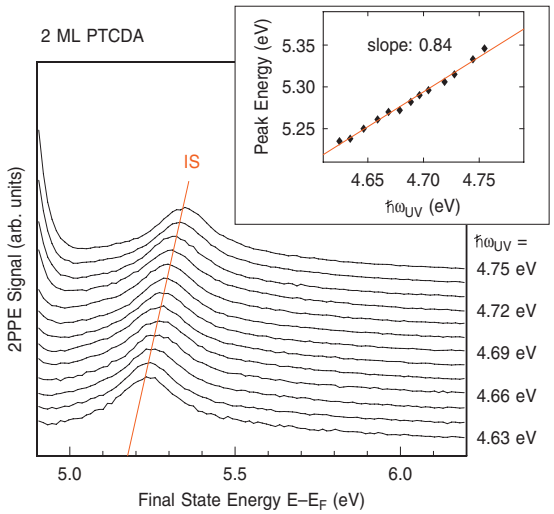

FIG. 4. Shift of IS with photon energy for a 2 ML film recorded with different photon energies. For higher photon energies the IS clearly shifts to higher final state energies. The inset shows the dependence of the peak positions (diamonds) on the photon energy together with a linear fit with a slope of 0.84.

width of the leading edge can be determined by taking the energetic distance between 10% and 90% of the rise. While for the clean substrate the width of 26 meV is limited mainly by the experimental resolution of the 2PPE system (22 meV, see Sec. II), this value increases to 36 meV for the 13 ML film [see Fig. 2(a)]. Hence an increasing inhomogeneity of the work function and consequently an increasing film roughness can be concluded. The generally relative sharp cutoff indicates a high quality of the investigated films.

C. Localization of the interface state and electron attenuation length

Figure 3 shows the 2PPE spectra for different PTCDA film thicknesses of a state, which has been identified as a Shockley-type IS in Ref. 10. The spectra are recorded at PE-I with similar experimental parameters to allow a direct comparison of the respective peak intensities: UV/UV excitation with $P_{UV}=1$ mW and $\hbar\omega_{UV}=4.69$ eV and with normal emission. From the attenuation of the peak with increasing film thickness, it is clear that the IS must be located at the PTCDA/Ag(111) interface. After a linear background was subtracted, the intensities of the peaks were determined by integrating over the energy range of $5.0\ \text{eV} < E - E_F < 5.6$ eV. The inset in Fig. 3 shows the thickness Θ dependent intensities $I(\Theta)$ plotted on a semilogarithmic scale. A fit with a simple exponential decay of the intensities $I = I_0 \exp(-\Theta/\lambda)$ yields an electron attenuation length of $\lambda = 2.9 \pm 0.6$ ML for the final state energy of 5.3 ± 0.1 eV. This corresponds to a length of $\lambda = (9.3 \pm 1.9)$ Å for a PTCDA interlayer spacing of 3.22 Å.[5]

The determined value for λ includes several uncertainties. For instance the thicknesses of the evaporated films are only known with an error of 0.5 ML. Also the films can roughen for higher coverages. However, the complete attenuation of the IS for films with thicknesses of more than 15 ML and the consistent results from the film thickness determination with XPS diminish this uncertainty to a large extent.

The characteristic dependence of the electron attenuation length on energy is usually described with the so-called universal curve.[30] For the material class of organic compounds, this curve yields an electron attenuation length of 3.7 ML PTCDA at an energy of 5.3 eV above E_F. The value of 2.9 ML determined here is slightly smaller than the respective attenuation length derived from the universal curve, but corresponds quite well to the literature value if the experimental error bar is considered. Moreover, for PTCDA a deviation of λ from the universal curve toward shorter attenuation lengths is possible at low energies.[31] This can be due to the variety of molecular vibrations[32] that constitute scattering channels for the electrons. Furthermore, at low energies the coupling of the excited electron wave function within the solid to the photoemission final state wave function in the vacuum may be ineffective due to selection rules. This can also decrease the attenuation length.

D. Dependence on photon energy

Figure 4 presents the dependence of the IS final state energy on photon energy. The spectra were recorded using UV/UV excitation with photon energies in the range of 4.63–4.75 eV. For increasing photon energies, the IS peak shifts to higher final state energies. The energetic position of the IS peak maximum shifts linearly with photon energy, as shown in the inset of Fig. 4. A linear fit of the peak final state energy change ΔE_{FS} versus photon energy variation $\Delta\hbar\omega$ reveals a shift of $\Delta E_{FS}/\Delta\hbar\omega = 0.84$. This shift is close to one, as expected for an unoccupied intermediate state and illustrated by the excitation scheme in Fig. 1. Within the time of the UV pulse, photons populate the IS with electrons from states below E_F, which are then excited into the vacuum in a

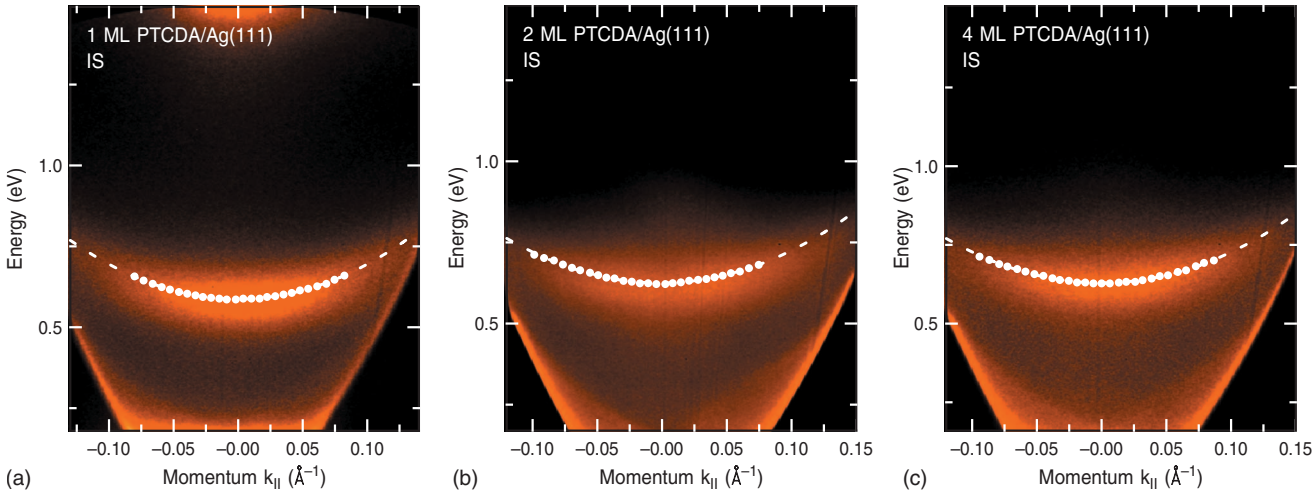

FIG. 5. Image of the dispersion of the IS at the $\bar{\Gamma}$-point for different PTCDA coverages recorded in the PE-II chamber with the two-dimensional detector. The PTCDA coverages are from left to right: $\Theta=1$ ML, $\Theta=2$ ML, and $\Theta=4$ ML.

second step. Consequently, the final state energy is the sum of the binding energy of the IS E_{IS} and the photon energy $\hbar\omega$.

The deviation of the shift $\Delta E_{FS}/\Delta\hbar\omega$ from one can have several reasons. First of all, the background changes with the photon energy. For higher photon energies more one photon processes from the proximity of E_F are possible, resulting in a strong increase in the background on the low energy end of the spectrum. This background does to some extent influence the evaluation of the peak position of the IS. Moreover, energetic resonances with other electronic states like e.g., molecular states, are likely. These resonances can be present at the initial state, intermediate state, or final state energy. The dependence of the peak shift on photon energy can be influenced by these resonances and hence deviate from one.

E. Dispersion of the interface state

The dispersion of an electronic state can directly be observed by means of the two-dimensional electron analyzer at the PE-II setup. Figure 5 presents the according IS dispersion data for PTCDA film thicknesses of $\Theta=1$ ML (left), $\Theta=2$ ML (center), and $\Theta=4$ ML (right). The intensity maxima of the dispersion curves are indicated by white dots. The parabolic fits to these maxima, shown as dashed curves in Fig. 5, reveal the energetic position at $\bar{\Gamma}$-point ($k_{\|}=0$) and the effective masses of the IS for the respective film thicknesses. For 1 ML the IS is located at (0.60 ± 0.01) eV above E_F and has an effective mass $m^{\star}=(0.36\pm0.04)m_e$. For 2 ML the state is at $E-E_F=(0.63\pm0.01)$ eV with $m^{\star}=(0.39\pm0.04)m_e$. For 4 ML the effective mass is $m^{\star}=(0.40\pm0.04)m_e$ without a significant change in the energy position. In comparison, the effective mass of the clean Ag(111) SS is $m^{\star}=0.40m_e$.[33] Additionally, Fig. 6(a) shows data for a 2 ML film, recorded with PE-I by varying the emission angle. Here, also spectra for higher $k_{\|}$ are shown. The spectra in Fig. 6(a) are normalized to their respective maximal signal. Overall, the signal diminishes for higher emission angles (see also Fig. 5), rendering a clear peak identification difficult for emission angles of more than 20°. The maxima of the IS, indicated by diamonds, show the same dispersion as the 2 ML data in Fig. 5 for small $k_{\|}$. For higher $k_{\|}$, however, a backfolding is observed that is not visible in Fig. 5 due to the limited range in $k_{\|}$. The 2 ML dispersion data are presented in Fig. 6(b) along with the 1 ML data[10] and the clean Ag(111) band structure.

Since the symmetry of the final state in photoemission is defined by the symmetry of the surface, it is altered if a superstructure is formed at the surface. Even bulk bands are expected to show backfolding due to Umklapp processes at the new SBZ boundaries of a commensurate superstructure.[35] This was observed, e.g., for the organic adsorbate system NTCDA/Au(111).[36] Backfolding of Shockley surface states was observed, e.g., upon reconstruction of the surface,[37,38] upon metal adsorption, e.g., for Ag/Cu(111),[39] and upon adsorption of noble gases, e.g., Xe/Cu(111).[40] In these cases, in addition to the backfolding, the influence of the periodic superstructure potential on the SS is expected to lead to the formation of energy gaps at the SBZ boundaries. Gaps of 69 meV were observed in photoemission spectra of the by ≈200 meV upshifted SS on Ag/Cu(111). For Xe/Cu(111) the gaps are expected to be in the unoccupied regime of the SS and therefore are not accessible to normal photoemission. In the chemisorbed system glycinate on Cu(100) a SS from the SBZ boundary is backfolded to the $\bar{\Gamma}$-point, due to the $p(2\times4)$ superstructure of the adlayer and could be observed by STS due to molecular orbital mediated tunneling.[41,42]

The fact that in the case of PTCDA/Ag(111) the IS is upshifted by $\Delta E=660$ meV compared to the SS on clean Ag(111) suggests a much stronger interaction than in the systems discussed above,[10] where generally a much smaller upshift is observed. Consequently, it is very likely that the scattering potentials defining the size of the gaps at the SBZ boundaries of the PTCDA/Ag(111) superlattice are large as well.

To further discuss backfolding of the IS we want to recapitulate the structure of PTCDA/Ag(111). The inset in Fig. 6(b) displays the herringbone arrangement of the PTCDA molecules within the monolayer on Ag(111). Due to the six-

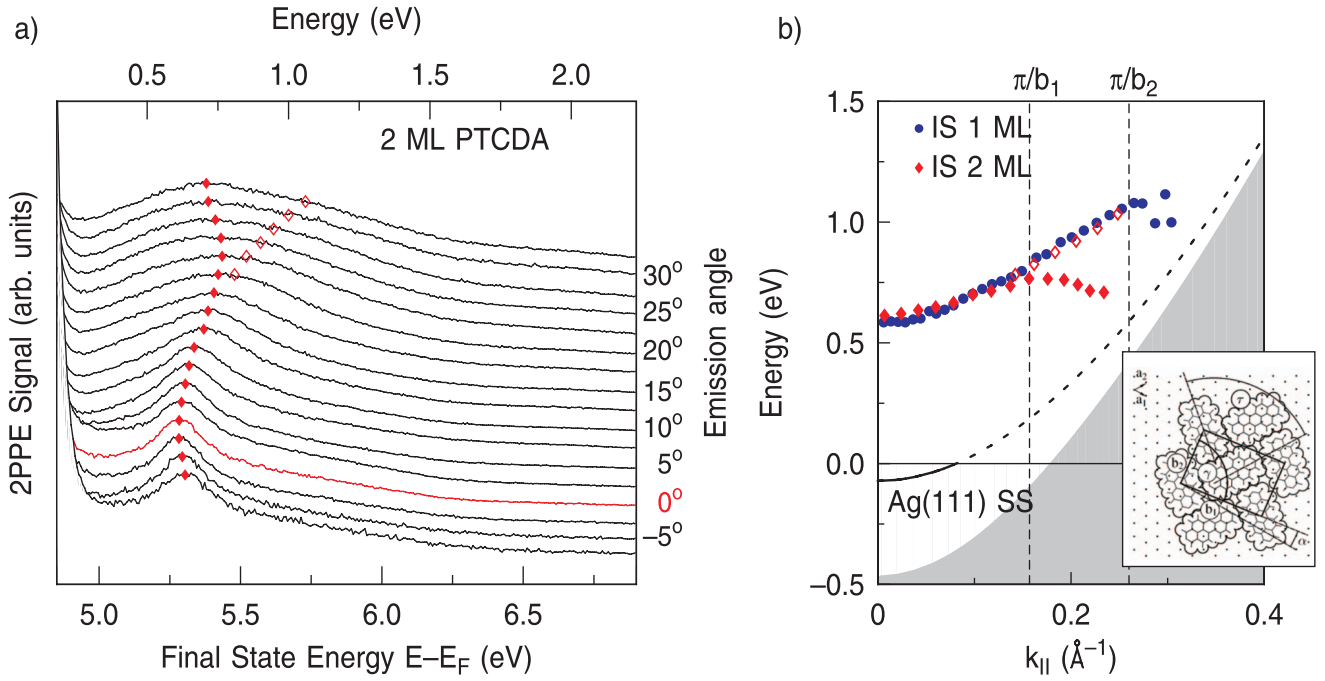

FIG. 6. (a) Emission angle dependent 2PPE spectra for 2 ML PTCDA/Ag(111). (b) IS dispersion for 1 and 2 ML samples of PTCDA/Ag(111). The lower *sp*-band and the SS data were extracted from Ref. 34. The PTCDA Brillouin zone boundaries are indicated by π/b_1 and π/b_2. The inset shows a sketch of the real space arrangement of the PTCDA molecules in the case of 1 ML on Ag(111). b_1 and b_2 are the long and short unit cell vectors of the PTCDA superstructure, respectively (from Ref. 8).

fold symmetry of the topmost substrate layer, the monolayer grows in six symmetry equivalent commensurate domains. This symmetry is conserved upon adsorption of the second layer. For the growth temperature of 270 K employed here, even additionally adsorbed layers have a sixfold symmetry.[8] Contrariwise, for films grown at 318 K, a coexistence of the α- and β-phase was observed and the growth from the third layer on is incommensurate due to the transition to the PTCDA bulk phases.[43]

The 2PPE spectra presented in Figs. 5 and 6 average over a large number of domains. The angle-resolved spectra thus consist of indistinguishable contributions from several differently oriented PTCDA unit cells that broaden the IS peak for increasing $k_\parallel$. This broadening is clearly observed in the angle-resolved spectra. However, as pointed out in Ref. 10, the monolayer data show a small gap at the SBZ boundary associated with the longer unit cell vector $\mathbf{b_1}(\pi/b_1)$ and a backfolding at the SBZ boundary which is generated by the shorter $\mathbf{b_2}(\pi/b_2)$. Additionally, backfolded intensity for $k_\parallel > \pi/b_1$ contributes to the broadening of the peak at the low energy side. In the 2 ML spectra presented in Fig. 6(a) the IS peak is even more broadened and backfolded at π/b_1. Also in this case, intensity can be tracked along the dispersion of the monolayer data for $k_\parallel > \pi/b_1$, indicated as open diamonds in Fig. 6. The differences in the backfolded intensities of the 1 and 2 ML spectra are supported by the observation that the electronic structure of the PTCDA monolayer and hence also the IS is altered upon adsorption of the second monolayer, e.g., indicated by the energy shift of the IS, see Fig. 3. In the dispersion spectra, particularly at large $k_\parallel$, these differences in the electronic structure apparently become more pronounced. Probably, the additional structural defects and the higher number of orientational domains in the second monolayer also contribute to the broadening of the IS peak. An increased scattering of the photoemitted electrons within the two PTCDA layers with only little energy exchange, e.g., scattering with phonons, can also lead to a broadened signal.

Furthermore, for higher emission angles the signal of the IS diminishes, probably due to selection rules. Likely, there are other electronic states such as nondispersive molecular states present in the investigated energy region. The signal of these states of multilayer molecules can be expected to increase for higher film thicknesses. Thus the broad features, presented in Fig. 6(a) for the 2 ML film, have probably contributions from such states and are not simply the IS and its backfolded intensity.

F. Momentum dependence of electron lifetime

In the last section, it was shown that the dispersion of the IS indicates backfolding at the PTCDA SBZ boundaries. Hence the question arises if the backfolding is related to a mixing of the IS with molecular states at least at large $k_\parallel$. In this context the dynamics of the excited IS can provide additional information. Especially the inelastic electron lifetime for higher $k_\parallel$ and accordingly for higher energies is interesting, where the IS band presumably crosses molecular states that have no or a small dispersion.

In order to study the dynamics of the monolayer IS, an excitation with the photon energy combination UV/blue was chosen. The disadvantage of slightly lower intensity of the blue laser compared to the IR laser is compensated by the energetic separation of the $n=1$ image-potential state peak and the IS (see Fig. 1). This is demonstrated in Fig. 7. For the UV/IR photon energy combination, the IS and $n=1$ peak

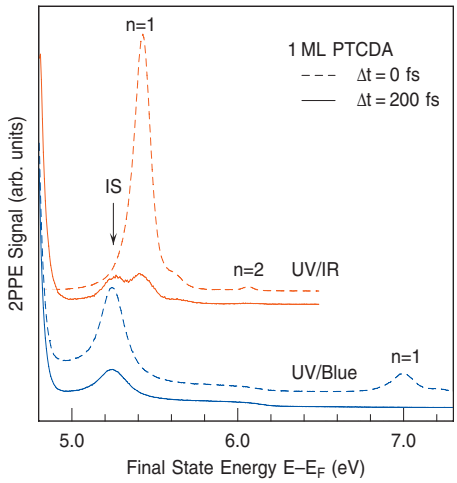

FIG. 7. Excitation of the IS with the photon energy combinations UV/IR (top) and UV/blue (bottom). Dashed lines show spectra at zero time delay and solid lines represent spectra at a delay of 200 fs.

are separated by only 200 meV resulting in one broad feature at $t=0$ fs that is dominated by the $n=1$ signal. Not until a time delay of 200 fs $n=1$ and IS signal are comparable. This renders time-resolved measurements difficult, because the contribution of the IS and $n=1$ to the time dependent signal have to be separated. This is especially difficult for short IS lifetimes. For the UV/blue photon energy combination the $n=1$ and IS are well separated in energy. However, with the UV/blue photon energy combination, the signal-to-noise ratio is inferior.

Figure 8 displays the inelastic lifetime of the IS for 1 and 2 ML films along the IS dispersion measured at the maximum of the IS peak with PE-I. The signal intensity of the 1 ML IS is plotted against the time delay between the blue pump- ($\hbar\omega_{\mathrm{Blue}}=3.01$ eV) and the UV probe-pulse ($\hbar\omega_{\mathrm{UV}}=4.70$ eV) in Fig. 8(a). For positive time delay a single exponential decay that accounts for the inelastic electron lifetime of the IS is clearly observable for each $k_{\parallel}$ data set. The time dependent intensities are fitted with a decay function consisting of the instrument response function (cross correlation) and a single exponential decay describing the inelastic lifetime of the IS. Along the IS dispersion, which is shown in Fig. 8(b), different exponential decay constants are observed. The fitted IS lifetimes τ_{IS} are shown in Fig. 8(c) along with analog measurements for a 2 ML film. The 1 ML inelastic lifetime of $\tau_{\mathrm{IS}}=50$ fs for $k_{\parallel}=0$ Å^{-1} decreases to 17 fs at 0.28 Å^{-1}. Up to a momentum of $k_{\parallel}=0.15$ Å^{-1}, the 2 ML film shows a similar behavior. For higher $k_{\parallel}$, where the 2 ML IS shows backfolding, the inelastic lifetime increases back to 44 fs at 0.22 Å^{-1}. Also, the decrease in the 1 ML IS inelastic lifetime levels off to some extent for $k_{\parallel}>0.25$ Å^{-1}, where this band shows backfolding.

The short inelastic lifetime of 50 fs at the IS band minimum indicates a decay of the excited electrons into the bulk metal.[10] During this *interband decay to the bulk*, the electron decays into the metal and transfers its energy and momentum to an electron-hole pair in bulk metallic states. For electrons with an energy above band bottom a second decay channel, *intraband scattering*, is present. In this process the electrons stay inside of the IS and relax in energy and momentum

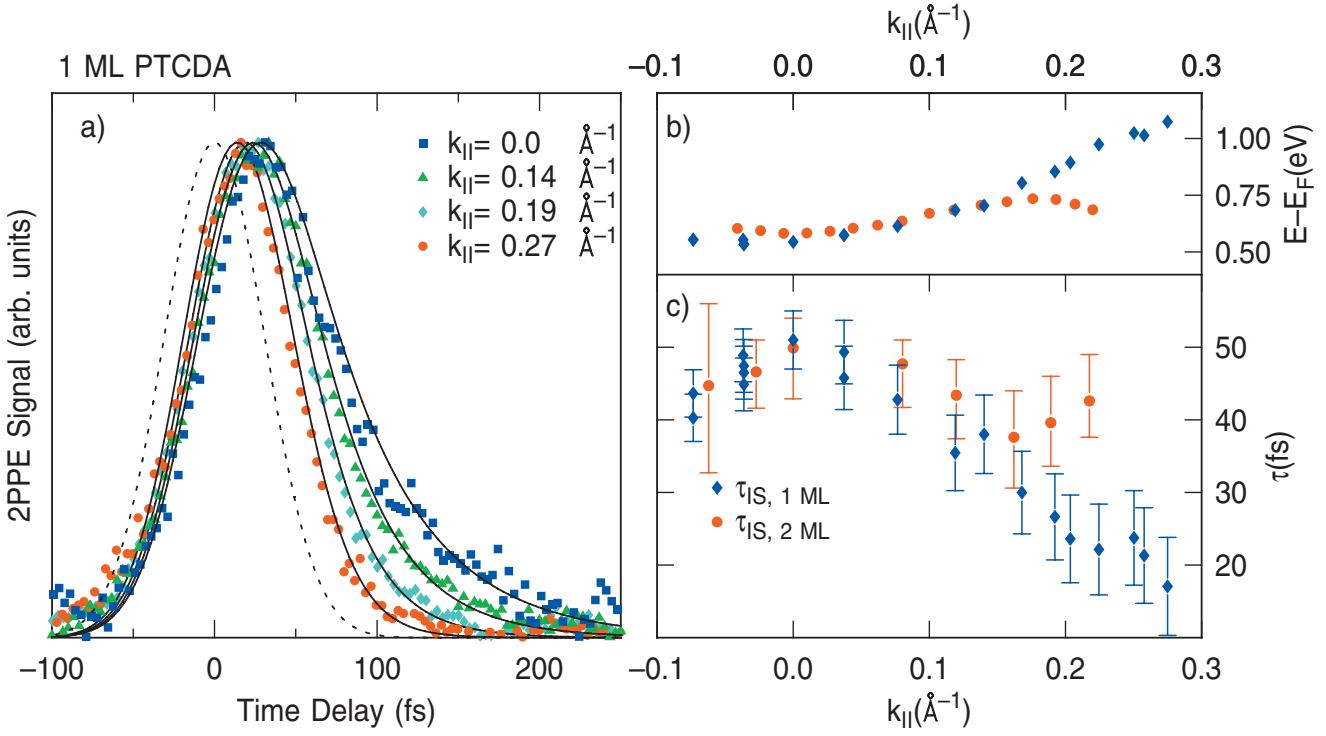

FIG. 8. Electron lifetime of the IS along the state's dispersion for PTCDA/Ag(111). (a) Two-color (UV/blue) 2PPE pump-probe traces of a 1 ML film of PTCDA/Ag(111) recorded at the IS maximum for different $k_{\parallel}$. The lifetimes are determined from a fit of an exponential decay at positive time delays (shown as black lines). The dashed line represents the cross correlation of the two laser pulses. (c) Lifetime of electrons excited into the IS for 1 and 2 ML along the IS band compared to the corresponding dispersion shown in (b).

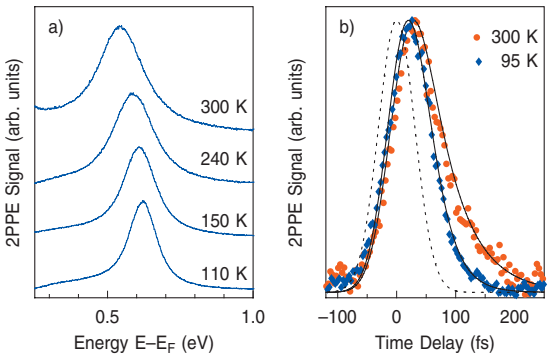

FIG. 9. (a) Comparison of the line shape of the IS for a 1 ML sample recorded at temperatures between 110 (bottom) and 300 K (top). (b) Time-resolved IS signal at temperatures of 95 and 300 K.

down to the band minimum. Here, energy and momentum are also transferred to the bulk metal.[44]

For the case of the IS, the details of these processes can only be explored by applying calculations that account for the exact wave functions along the IS band and their bulk penetration. However, certain trends can be expected.[44] First, the inelastic lifetime of excited electrons is generally dependent on the wave function overlap of the initial state (before the decay) and the final state (after the decay). Specifically, the decay rate $\Gamma=\hbar/\tau$ depends linearly on this wave function overlap. For interband decay to the bulk the wave function overlap is expected to be smaller than for decay due to intraband scattering, where initial and final state wave function are both the IS wave functions, differing only in parallel momentum $k_{\|}$. Second, the decay rate is expected to increase with transferred energy between initial and final state due to an increasing phase space for inelastic electron hole pair decay and to decrease with exchanged momentum. Eventually, the decrease in the inelastic lifetime for increasing $k_{\|}$ is caused on the one hand by the additional intraband scattering and on the other hand by the increased energy, rendering both intraband scattering and interband decay to the bulk more efficient.

The inelastic lifetimes of electrons excited into the backfolded bands, especially for the 2 ML case are substantially larger than the inelastic lifetimes of electrons in the 1 ML data with the same momentum. This indicates different decay mechanisms in the backfolded band than in the parabolalike band of the 1 ML data. These decay mechanisms could be an indication for the influence of the molecule on the IS electronic structure.

G. Temperature dependence of linewidth and lifetime

More information yields the comparison of the linewidth of the IS on the one hand and the decay rates on the other hand. In Fig. 9(a) IS spectra are shown for temperatures between 110 and 300 K. Two characteristics are evident. First, the linewidth clearly increases with temperature. At 300 K the 2PPE linewidth (180 meV) is more than a factor of 10 larger than the decay rate (13 meV). This might be an indication for a contribution of quasielastic scattering to the linewidth.[45,46] If the temperature dependence of the full width at half maximum (FWHM) linewidths are evaluated using the linear relation $\Gamma=\Gamma_0+2\Gamma^{\star}$ with $\Gamma^{\star}=2\pi\lambda_{\text{e-ph}}k_BT$, an electron-phonon coupling parameter $\lambda_{\text{e-ph}}=0.3\pm0.1$ can be determined. The error for the determined coupling constant is estimated to be 0.1, due to the difficulty to subtract the appropriate background from the peaks before determination of the FWHM. Second, the IS peak shifts from $E-E_F=0.62$ eV at 110 K to 0.54 eV at 300 K. This suggests a change in at least the electronic structure but likely also of the peculiar adsorption structure of the molecules. At elevated temperatures a reduced interaction of the molecules with the metal is possible that could be caused by excited anharmonic out-of-plane molecular vibrations or an increased lattice mismatch between the metal and the molecular layer. If the distance between the molecules and the metal surface is actually smaller for low temperatures, as it was at least observed for the PTCDA low temperature phase,[47] this would directly cause a further shift of the IS wave function into the metal and consequently a shift to higher energy and a reduced lifetime. A change in electronic structure could also have a profound influence on the peak structure, like, e.g., a temperature dependent Gaussian contribution that was not accounted for in the determination of $\lambda_{\text{e-ph}}$. A change in the electronic structure with temperature is supported by the temperature dependence of the inelastic lifetime. Figure 9(b) shows blue/UV pump-probe traces for temperatures of 300 and 95 K. The inelastic lifetime diminishes from 53 fs at 300 K to 28 fs at 95 K. This can only be explained by a change in the electronic structure since the inelastic lifetime should increase with lower temperature.

Compared to our estimation of $\lambda_{\text{e-ph}}$ for the IS, the Ag(111) SS has a coupling parameter $\lambda_{\text{e-ph}}=0.12$.[48] However, HREELS spectra of PTCDA monolayers on Ag(111) showed strong electron-phonon coupling[32] and valence hole-molecular vibration coupling is observed in a large number of similar systems.[49] For PTCDA/Ag(111) the electron-phonon coupling was associated with the coupling of two PTCDA breathing modes to the dynamic charge transfer between the Ag(111) substrate and the PTCDA monolayer. If the IS electron-phonon coupling parameter is interpreted as a measure for the entire system, including all molecular vibrations and phonons in the metal substrate, the higher value of $\lambda_{\text{e-ph}}=0.3$, compared to the Ag(111) SS value, might be reasonable.

IV. CONCLUSION

In this paper we studied the electronic structure of the PTCDA/Ag(111) interface systematically by means of 2PPE. Especially the access to a flexible excitation laser system with a variety of applicable wavelengths is a significant experimental advantage. First, the UV laser with a photon energy just below the sample workfunction can probe unoccupied states even close to the Fermi level. Second, with the ability to choose between UV, IR, blue, and green laser pulses, different excitation schemes are available that allow us to separate the respective peaks in the spectra. Third, the two color setup allows us to reliably distinguish different states in time-resolved measurements.

The Shockley-type IS can be characterized as a predomi-

nant metal state at the $\bar{\Gamma}$-point with a possible increasing molecular character for higher $k_{\|}$. This is indicated by the backfolding and peak broadening in the dispersion data and by the $k_{\|}$-dependence of the inelastic lifetime. A comparison of the inelastic lifetime of the IS with its peak linewidth hints to a significant electron-phonon coupling. The temperature dependence of the inelastic lifetime and the peak position of the IS suggest slight variations in the electronic structure of the PTCDA monolayer grown at room temperature.

Summarizing our results, the IS complements the chemisorption picture of PTCDA/Ag(111). It contributes to the static charge transfer at the interface. Furthermore, the IS wave function extends across the interface. The IS is also sensitive to the adsorption of a second monolayer. This is evident from the change in its properties in the 2 ML system. With a change in its binding energy at the $\bar{\Gamma}$-point, the effective electron mass increases. At the same time, the backfolding at high $k_{\|}$ is altered, and the inelastic lifetime of the IS slightly increases. These observations corroborate the influence of the second monolayer on the first monolayer electronic structure, which is, e.g., evident in UPS.[4] Moreover, additional interesting properties of the PTCDA/Ag(111) system could be studied in detail with 2PPE. Very small variations in the work function in the range of 1–10 ML could be revealed and the electron attenuation length was determined for very low energy photoelectrons.

ACKNOWLEDGMENTS

We thank S. Krause, F. Forster, J. Güdde, F. S. Tautz, and R. Temirov for fruitful discussions. We acknowledge funding by the Deutsche Forschungsgemeinschaft through Grant Nos. SPP1093, SPP1121, GK790, and GK1221. One of us (E.U.) thanks the Fonds der Chemischen Industrie for support.

[1] X.-Y. Zhu, Surf. Sci. Rep. **56**, 1 (2004).
[2] E. Umbach, C. Seidel, J. Taborski, R. Li, and A. Soukopp, Phys. Status Solidi B **192**, 389 (1995).
[3] I. Hill, A. Rajagopal, A. Kahn, and Y. Hu, Appl. Phys. Lett. **73**, 662 (1998).
[4] Y. Zou, L. Kilian, A. Schöll, T. Schmidt, R. Fink, and E. Umbach, Surf. Sci. **600**, 1240 (2006).
[5] F. S. Tautz, Prog. Surf. Sci. **82**, 479 (2007).
[6] M. Rohlfing, R. Temirov, and F. S. Tautz, Phys. Rev. B **76**, 115421 (2007).
[7] H. Marchetto, U. Groh, T. Schmidt, R. Fink, H.-J. Freund, and E. Umbach, Chem. Phys. **325**, 178 (2006).
[8] L. Kilian, E. Umbach, and M. Sokolowski, Surf. Sci. **573**, 359 (2004).
[9] R. Temirov, S. Soubatch, A. Luican, and F. S. Tautz, Nature (London) **444**, 350 (2006).
[10] C. H. Schwalb, S. Sachs, M. Marks, A. Schöll, F. Reinert, E. Umbach, and U. Höfer, Phys. Rev. Lett. **101**, 146801 (2008).
[11] A. Yang, S. T. Shipman, S. Garrett-Roe, J. Johns, M. Strader, P. Szymanski, E. Muller, and C. Harris, J. Phys. Chem. C **112**, 2506 (2008).
[12] R. Haight, Surf. Sci. Rep. **21**, 275 (1995).
[13] M. Weinelt, M. Kutschera, T. Fauster, and M. Rohlfing, Phys. Rev. Lett. **92**, 126801 (2004).
[14] T. Ichibayashi and K. Tanimura, Phys. Rev. B **75**, 235327 (2007).
[15] M. Mauerer, I. L. Shumay, W. Berthold, and U. Höfer, Phys. Rev. B **73**, 245305 (2006).
[16] M. Wolf, E. Knoesel, and T. Hertel, Phys. Rev. B **54**, R5295 (1996).
[17] M. Bauer, S. Pawlik, and M. Aeschlimann, Phys. Rev. B **60**, 5016 (1999).
[18] U. Höfer, I. Shumay, C. Reuß, U. Thomann, W. Wallauer, and T. Fauster, Science **277**, 1480 (1997).
[19] J. Güdde, M. Rohleder, T. Meier, S. W. Koch, and U. Höfer, Science **318**, 1287 (2007).
[20] A. Winkelmann, F. Bisio, R. Ocana, W. C. Lin, M. Nyvlt, H. Petek, and J. Kirschner, Phys. Rev. Lett. **98**, 226601 (2007).
[21] C. Harris, N.-H. Ge, R. Lingle, Jr., J. McNeill, and C. Wong, Annu. Rev. Phys. Chem. **48**, 711 (1997).
[22] J. Stahler, C. Gahl, U. Bovensiepen, and M. Wolf, J. Phys. Chem. B **110**, 9637 (2006).
[23] J. Güdde, W. Berthold, and U. Höfer, Chem. Rev. (Washington, D.C.) **106**, 4261 (2006).
[24] B. Li, J. Zhao, K. Onda, K. D. Jordan, J. L. Yang, and H. Petek, Science **311**, 1436 (2006).
[25] A. G. Borisov, V. Sametoglu, A. Winkelmann, A. Kubo, N. Pontius, J. Zhao, V. M. Silkin, J. P. Gauyacq, E. V. Chulkov, P. M. Echenique, and H. Petek, Phys. Rev. Lett. **101**, 266801 (2008).
[26] M. Rohleder, K. Duncker, W. Berthold, J. Güdde, and U. Höfer, New J. Phys. **7**, 103 (2005).
[27] J. Güdde and U. Höfer, Prog. Surf. Sci. **80**, 49 (2005).
[28] H. Ishii, K. Sugiyama, E. Ito, and K. Seki, Adv. Mater. (Weinheim, Ger.) **11**, 605 (1999).
[29] G. Witte, S. Lukas, P. S. Bagus, and C. Wöll, Appl. Phys. Lett. **87**, 263502 (2005).
[30] M. P. Seah and W. A. Dench, Surf. Interface Anal. **1**, 2 (1979).
[31] T. Graber, A. Schöll, E. Umbach, and F. Reinert (unpublished).
[32] F. S. Tautz, M. Eremtchenko, J. A. Schaefer, M. Sokolowski, V. Shklover, and E. Umbach, Phys. Rev. B **65**, 125405 (2002).
[33] F. Reinert, G. Nicolay, S. Schmidt, D. Ehm, and S. Hüfner, Phys. Rev. B **63**, 115415 (2001).
[34] M. Becker, S. Crampin, and R. Berndt, Appl. Phys. A: Mater. Sci. Process. **88**, 555 (2007).
[35] J. Anderson and G. J. Lapeyre, Phys. Rev. Lett. **36**, 376 (1976).
[36] J. Ziroff, P. Gold, A. Bendounan, F. Forster, and F. Reinert, Surf. Sci. **603**, 354 (2009).
[37] F. Reinert and G. Nicolay, Appl. Phys. A: Mater. Sci. Process. **78**, 817 (2004).
[38] D. Malterre, B. Kierren, Y. Fagot-Revurat, S. Pons, A. Tejeda, C. Didiot, H. Cercellier, and A. Bendounan, New J. Phys. **9**, 391 (2007).
[39] A. Bendounan, F. Forster, J. Ziroff, F. Schmitt, and F. Reinert, Phys. Rev. B **72**, 075407 (2005).
[40] F. Forster, S. Hüfner, and F. Reinert, J. Phys. Chem. B **108**, 14692 (2004).
[41] K. Kanazawa, Y. Sainoo, Y. Konishi, S. Yoshida, A. Taninaka, A. Okada, M. Berthe, N. Kobayashi, O. Takeuchi, and H. Shigekawa, J. Am. Chem. Soc. **129**, 740 (2007).
[42] M. S. Dyer and M. Persson, J. Phys.: Condens. Matter **20**, 312002 (2008).
[43] B. Krause, A. C. Dürr, K. Ritley, F. Schreiber, H. Dosch, and D. Smilgies, Phys. Rev. B **66**, 235404 (2002).
[44] W. Berthold, U. Höfer, P. Feulner, E. V. Chulkov, V. M. Silkin, and P. M. Echenique, Phys. Rev. Lett. **88**, 056805 (2002).
[45] Ch. Reuß, I. L. Shumay, U. Thomann, M. Kutschera, M. Weinelt, Th. Fauster, and U. Höfer, Phys. Rev. Lett. **82**, 153 (1999).
[46] E. Knoesel, A. Hotzel, and M. Wolf, Phys. Rev. B **57**, 12812 (1998).
[47] L. Kilian, A. Hauschild, R. Temirov, S. Soubatch, A. Schöll, A. Bendounan, F. Reinert, T. L. Lee, F. S. Tautz, M. Sokolowski, and E. Umbach, Phys. Rev. Lett. **100**, 136103 (2008).
[48] A. Eiguren, B. Hellsing, E. V. Chulkov, and P. M. Echenique, Phys. Rev. B **67**, 235423 (2003).
[49] S. Kera, H. Yamane, and N. Ueno, Prog. Surf. Sci. **84**, 135 (2009).